Published in final edited form as:
Magn Reson Med. 2008 August ; 60(2): 479–484. doi:10.1002/mrm.21692.

Fat-Water Separation with Alternating Repetition Time Balanced SSFP

Tolga Çukur[1] and **Dwight G. Nishimura**[1]

[1]Magnetic Resonance Systems Research Laboratory, Department of Electrical Engineering, Stanford University, Stanford, California

Abstract

Balanced SSFP achieves high SNR efficiency, but suffers from bright fat signal. In this work, a multiple-acquisition fat-water separation technique using alternating repetition time (ATR) balanced SSFP is proposed. The SSFP profile can be modified using alternating repetition times and appropriate phase cycling to yield two spectra where fat and water are in-phase and out-of-phase respectively. The signal homogeneity and the broad width of the created in-phase and out-of-phase profiles lead to signal cancellation over a broad stop-band. The stop-band suppression is achieved for a wide range of flip angles and tissue parameters. This property, coupled with the inherent flexibility of ATR SSFP in repetition time selection, makes the method a good candidate for fat-suppressed SSFP imaging. The proposed method can be tailored to achieve a smaller residual stop-band signal or a decreased sensitivity to field inhomogeneity depending on application-specific needs.

Keywords

SSFP; alternating repetition time; fat-water separation; fat suppression; in-phase and out-of-phase

Introduction

Fully-refocused steady-state free precession (SSFP) imaging (1-3) (also known as balanced SSFP, FIESTA, TrueFISP), provides high signal-to-noise ratio (SNR) efficiency. However, the T1/T2 dependence of the SSFP signal causes fat tissue to appear bright in the reconstructed images. The tissues of interest usually have a comparable or smaller balanced SSFP signal. Therefore, fat-water separation or fat suppression methods have commonly been coupled with SSFP imaging to improve depiction of the structures of interest.

A number of interesting strategies have been devised for reducing or suppressing the fat signal. The transient SSFP signal can be manipulated during the course of acquisition (4,5). However, transient signal oscillations may lead to artifacts (6), 3D imaging is difficult, and images can be blurred due to overweighting of the central part of k-space. The phase difference due to the chemical-shift between fat and water can be used to separate the two components using single and multiple acquisition techniques (7,8), though for these techniques, partial volume effects lead to estimation errors.

A variety of effective SSFP fat suppression methods reduce the fat signal by creating a stop-band around the fat-resonance (9-14). Linear combination SSFP (LCSSFP) (10) uses two

Address correspondence to: Tolga Çukur, Packard Electrical Engineering, Room 210, 350 Serra Mall, Stanford, CA 94305-9510, TEL: (650) 725-7005, E-MAIL: cukur@stanford.edu .

separate phase-cycled acquisitions and combines them to yield a spectral stop-band around the fat-resonance. The width of the stop-band and the separation between the pass- and the stop-band are determined by the repetition time (TR). On the other hand, alternating repetition time (ATR) SSFP (14) can create a broad stop-band by aligning the spins precessing at the fat-resonance back to the longitudinal axis. LCSSFP puts stringent limitations on the optimal repetition times, whereas fat-suppressing (FS) ATR SSFP allows for a broader range of repetition times without significantly increasing the sensitivity to homogeneity.

We propose a fat-water separation method comprising in-phase and out-of-phase ATR SSFP images. The individual ATR SSFP spectra are flatter compared to regular balanced SSFP, and the in-phase and out-of-phase profiles are nearly identical to each other. Therefore, the proposed method creates a wide stop-band with a small amount of remnant signal and an increased immunity to field inhomogeneity. The inherent flexibility of ATR in the selection of the repetition time allows for a greater range of parameter prescriptions. A number of fat-suppressed SSFP imaging applications may benefit from this technique such as musculoskeletal imaging (15), coronary artery imaging (16), and peripheral and renal angiography (17,18).

Theory

Alternating TR SSFP uses two separate repetition times, TR1 and TR2, consecutively. The RF excitations, RF1 and RF2 (at the beginning of periods of duration TR1 and TR2), have the same flip angle. Assuming only the TR1-period is used for acquiring data and TR2 is relatively short, the main task for this second period is changing the shape of the frequency response to create a stop-band with an appropriate phase-cycling scheme (14). The magnetization at the frequency of the stop-band null should be longitudinal during the acquisition period (TR1). Following the terminology in Ref. 14, the resulting relationship between the repetition times and the phase of the second RF pulse (ψ_2) is,

$$\psi_2 = 360^\circ \tau / (\tau + 1), \quad (1)$$

where τ = TR2/TR1. Fat suppression can be achieved if the separation between the centers of the pass- and the stop-band determined by 1/(TR1+TR2) equals the frequency shift between fat and water. At 1.5 T, this corresponds to the following condition,

$$TR1 + TR2 = 4.6 ms. \quad (2)$$

The phase of the signal has 180° jumps across the signal nulls inherent in SSFP sequences. Furthermore, there is a null at the center of the stop-band and another at the transition from the stop-band to the pass-band. As a result, the signal for frequencies to the right of the stop-band null is out-of-phase with the pass-band signal. On the other hand, the signal for the frequencies to the left of the stop-band null is in-phase with the pass-band signal. Since the location of the stop-band null can be adjusted by changing ψ_2, the in-phase or out-of-phase portions can be selectively extended.

If the stop-band null is shifted to the boundary between the pass- and stop-bands; i.e., halfway between the water and fat resonances (approximately -110 Hz at 1.5 T), by decreasing ψ_2, the entire band around the fat-resonance becomes in-phase with the on-resonance water signal. On the other hand, increasing ψ_2 creates an equal amount of shift in the other direction (to -330 Hz at 1.5 T) and yields a fat signal out-of-phase with the water signal. It is important to note that changing ψ_2 affects the shape of the stop-band profile and

turns it into a relatively flat pass-band. The exact values for the phase of the second RF pulse that yield the desired signal profiles are,

$$\psi_2^{i,o}=\begin{cases} 180^\circ\tau/(1+\tau) & , \text{ for in-phase fat signal,} \\ 540^\circ\tau/(1+\tau) & , \text{ for out-of-phase fat signal.} \end{cases} \quad (3)$$

The resulting in-phase $\left(\psi_2^i=45^\circ\right)$ and out-of-phase $\left(\psi_2^o=135^\circ\right)$ magnetization profiles for α = 60°, TR1/TR2/TE = 3.45/1.15/1.725 ms and T1/T2 = 1000/200 ms (for arterial blood) are displayed in Fig. 1.a. It is important to note that there is a phase difference between the pass-band signal of the different profiles. This phase difference does not depend on the flip angle and T1/T2 of the tissue. Therefore, it is a constant number for a given prescription of sequence parameters. The water-only image can be obtained by a summation of the in-phase and out-of-phase profiles after the compensation of this phase difference. Similarly, a subtraction following this compensation yields the fat image. The water-only and fat-only spectra are shown in Fig. 1.b. A bSSFP sequence has a symmetric steady-state because subsequent precession intervals (TRs) are identical. However, the inherent asymmetry in ATR SSFP allows for a greater amount of precession in TR1 without creating a signal null (19), resulting in a broader and flatter pass-band. The cancellation of the fat signal in the stop-band is due to this flat shape of the in-phase and out-of-phase magnetization profiles.

Looking at Fig. 1.b, it can be observed that the fat-only profile can also be used for fat-suppression if the center of the pass-band for the fat-only spectrum is shifted to the water-resonance. This shift can be achieved by changing the phase of the second RF pulse:

$$\psi_2^{i,o}=\begin{cases} 180^\circ\tau/(1+\tau) & , \text{ for in-phase fat signal,} \\ -180^\circ\tau/(1+\tau) & , \text{ for out-of-phase fat signal.} \end{cases} \quad (4)$$

The resulting in-phase $\left(\psi_2^i=45^\circ\right)$ and out-of-phase $\left(\psi_2^o=-45^\circ\right)$ magnetization profiles are displayed in Fig. 1.c. The water-only and fat-only spectra are shown in Fig. 1.d. At the expense of a 10.52 percent reduced signal compared with the $\psi_2^{i,o}=(45^\circ, 135^\circ)$ pair, the water-only profile for the $\psi_2^{i,o}=(45^\circ, -45^\circ)$ pair has a broad stop-band with approximately 1/τ times the width of the pass-band.

The proposed method offers flexibility in the selection of the parameters TR1 and TR2 as it is based on ATR-SSFP. In addition, a range of total TR (TR1+TR2) values can be prescribed without significantly compromising the stop-band suppression. As the total TR is increased, the widths of the stop- and pass-bands (α 1/(*TR*1 + *TR*2)) will be smaller. The center of the profile (midway between the centers of the pass- and stop-bands) can be aligned with a point halfway between the fat- and water-resonances. Given the fat-water frequency separation $\Delta f_{fat\text{-}water}$ (< 0), the resulting frequency shift Δf is:

$$\Delta f=\frac{|\Delta f_{\text{fat-water}}|-1/(TR1+TR2)}{2}. \quad (5)$$

Equivalently the phase of the RF1 and RF2 pulses can be selected to yield the desired frequency shift. The following terms should be added to the phase increment between the RF1 pulses (ϕ_1) and the RF2 pulses $\left(\psi_2^{i,o}\right)$ respectively:

$$\Delta\phi_1 = -360^\circ\,(TR1+TR2)\,\Delta f, \tag{6}$$

$$\Delta\psi_2 = -360^\circ\,(TR1)\,\Delta f. \tag{7}$$

The similarity between the in- and out-of-phase profiles over the fat-resonance is higher for the $\psi_2^{i,o} = (45^\circ, 135^\circ)$ pair. As a result, the stop-band suppression of this pair is more robust than that of the $\psi_2^{i,o} = (45^\circ, -45^\circ)$ pair. On the other hand, the $\psi_2^{i,o} = (45^\circ, -45^\circ)$ pair has a slightly broader pass-band and a very broad stop-band. Therefore, there is a trade-off between the broadness of the bands and the level of stop-band suppression, comparing the two pairs. If the stop-band width of the $\psi_2^{i,o} = (45^\circ, 135^\circ)$ pair is enough, it will yield better suppression. In contrast, the increased band-broadness of the latter pair achieves more robust fat-suppression in the presence of high field-inhomogeneities, at higher field strengths, or with longer TR1+TR2.

The increased frequency separation between fat and water at 3 T would suggest the use of TR1+TR2 = 2.3 ms for the $\psi_2^{i,o} = (45^\circ, 135^\circ)$ pair. If this constraint cannot be satisfied, then TR1 (3.45 ms) and TR2 (1.15 ms) can be kept the same while the frequency responses of the in- and out-of-phase profiles are shifted to align the stop-band with the fat-resonance (approximately -440 Hz at 3 T). Leupold et al. proposed using $\psi_2 = 180°$ to achieve this alignment for the FS-ATR profile (14). Similarly, adding 90° to the original $\psi_2^{i,o} = (45^\circ, 135^\circ)$ pair -such that $\psi_2^{i,o} = (135^\circ, 225^\circ)$- shifts the stop-band to the desired location. The profile for the $\psi_2^{i,o} = (45^\circ, -45^\circ)$ pair already has a stop-band around the fat-resonance; therefore, no change in the phase cycling scheme is required.

Methods

The average remnant stop-band signal compared to the pass-band signal can serve as an appropriate measure for the effectiveness of the stop-band suppression. This measure can be used to analyze the robustness of the method to variations in tissue and scan parameters, and to allow a fair comparison between different methods. Simulations were performed to compute the ratio of the average pass-band signal (±80 Hz around the water-resonance) to the average stop-band signal (±80 Hz around the fat-resonance) for two different flip angles (α = 30° and 60°), a broad range of T1/T2 ratios (1 to 10) to be found in vivo, and a practically useful range of TR2/TR1 (τ) ratios (0.2 to 0.5, while TR1+TR2 = 4.6 ms). The pass-band to stop-band signal ratios were simulated for LCSSFP, FS-ATR, and the proposed method. For LCSSFP, TR = 2.3 ms and TE = 1.15 ms were assumed. For FS-ATR and the proposed method TR1 = 3.45 ms, TR2 = 1.15 ms and TE = 1.725 ms were used.

To verify the proposed method, 3D images of a water bottle were acquired with the following scan parameters: α = 60°, TR1/TR2/TE = 3.45/1.15/1.7 ms, 2 mm isotropic resolution, ±125 kHz BW. A linear field gradient was applied along the readout direction to generate spatially varying precession frequency. Two sets of in-phase and out-of-phase images were acquired, corresponding to the $\psi_2^{i,o} = (45^\circ, 135^\circ)$ and $\psi_2^{i,o} = (45^\circ, -45^\circ)$ pairs.

Calf images were acquired with a 3D ATR SSFP sequence on 1.5 T and 3 T GE Signa Excite scanners. At 1.5 T, the $\psi_2^{i,o} = (45^\circ, 135^\circ)$ and FS-ATR (ψ_2 = 90°) methods were

compared. The only parameters changed from the phantom acquisition were an FOV of 26 cm, an isotropic resolution of 1 mm and a total acquisition time of 2:30 for the $\psi_2^{i,o} = (45^\circ, 135^\circ)$ pair. To demonstrate fat suppression at high field, the same 3D ATR SSFP sequence prescription was used. The $\psi_2^{i,o} = (135^\circ, 225^\circ)$, $\psi_2^{i,o} = (45^\circ, -45^\circ)$ and FS-ATR (ψ_2 = 180°) methods were compared.

LCSSFP images acquired at 1.5 T were also compared with the $\psi_2^{i,o} = (45^\circ, 135^\circ)$ and $\psi_2^{i,o} = (45^\circ, -45^\circ)$ methods. The aforementioned 3D ATR SSFP sequence was used with the same parameters. The LCSSFP sequence used the same scan parameters except for TR = 3.3 ms and TE = 1.45 ms.

Three volunteers were scanned for the experiments performed at 1.5 T, whereas data from a single volunteer is presented for the 3 T study. IRB consent was obtained from all subjects. Quantitative analysis of the level of fat suppression was performed by computing the highest fat-to-muscle contrast-to-noise ratio (CNR) and contrast observed in an image. On the other hand, blood-to-muscle CNR and contrast were used to quantify the loss in blood vessels. The measurements from all volunteers were averaged.

Results

The pass-band to stop-band signal ratio was computed for the $\psi_2^{i,o} = (45^\circ, 135^\circ)$ and $\psi_2^{i,o} = (45^\circ, -45^\circ)$ combinations. The flatness of the in-phase and out-of-phase profiles increases with higher flip angles, yielding better stop-band suppression. The highest level of suppression is achieved for τ within the range [0.25 0.4]. On the other hand, the sensitivity of the ratio to T1/T2 is very low. The stop-band suppression for the $\psi_2^{i,o} = (45^\circ, -45^\circ)$ combination is lower; however, the increased stop-band width will yield improved suppression with high field-inhomogeneities.

The average pass-band to stop-band signal ratios for FS-ATR, LCSSFP, and the proposed methods are compared in Fig. 2. All methods are relatively insensitive to the T1/T2 ratio; however, they display a stronger flip-angle dependency. The stop-band suppression of the single-acquisition FS-ATR method is less effective than the multiple-acquisition methods considered. As predicted by the previous simulation, the performance of the proposed method improves at higher flip angles. The sequence of $\psi_2^{i,o} = (45^\circ, 135^\circ)$ outperforms LC-SSFP for the whole range of flip angles and tissue parameters except for a small vicinity around α = 30°. Furthermore, for optimal performance LCSSFP restricts the TR to 2.3 ms, whereas the proposed method does not place stringent limitations on TR.

The fat-suppressed phantom images for the $\psi_2^{i,o} = (45^\circ, 135^\circ)$ and $\psi_2^{i,o} = (45^\circ, -45^\circ)$ combinations are shown in Fig. 3, where the wide stop-bands yield a minimal remnant signal. The $\psi_2^{i,o} = (45^\circ, -45^\circ)$ combination creates a broader stop-band as predicted.

Figures 4.a shows axial and coronal slices along with the corresponding maximum-intensity-projections (MIPs) for the FS-ATR (ψ_2 = 90°) and $\psi_2^{i,o} = (45^\circ, 135^\circ)$ acquisitions at 1.5 T. The proposed method achieves greater suppression than FS-ATR as shown by the superior vessel depiction in the MIPs. There are regions with visible residual fat as a result of the remnant stop-band signal in the water images reconstructed with the proposed method. It is

important to note that the $\psi_2^{i,o} = (45^\circ, -45^\circ)$ pair would not improve the level of suppression, as these regions are within the stop-band width of the $\psi_2^{i,o} = (45^\circ, 135^\circ)$ pair.

Sagittal and coronal thin slab MIPs of the 3 T calf images are shown in Fig. 4.b for the FS-ATR ($\psi_2 = 180°$), $\psi_2^{i,o} = (135^\circ, 225^\circ)$ and $\psi_2^{i,o} = (45^\circ, -45^\circ)$ methods. Both multiple-acquisition methods achieve better fat suppression than FS-ATR; however, the field inhomogeneity limits the performance of the $\psi_2^{i,o} = (135^\circ, 225^\circ)$ combination. On the other hand, the broader stop-band achievable with the $\psi_2^{i,o} = (45^\circ, -45^\circ)$ pair yields improved fat suppression with minimal remnant fat signal.

Figure 5 displays sagittal and axial slices for the LCSSFP, $\psi_2^{i,o} = (45^\circ, 135^\circ)$ and $\psi_2^{i,o} = (45^\circ, -45^\circ)$ acquisitions at 1.5 T. The field inhomogeneity limits the level of fat suppression with the LCSSFP and $\psi_2^{i,o} = (45^\circ, 135^\circ)$ methods. In contrast, the broad stop-band of the $\psi_2^{i,o} = (45^\circ, -45^\circ)$ pair yields improved fat suppression.

The mean fat-to-muscle (CNR, contrast) measurements among the subjects for the studies conducted at 1.5 T were as follows: (15.73, 3.77) for FS-ATR, (28.02, 4.03) for LC-SSFP, (10.58, 2.31) for $\psi_2^{i,o} = (45^\circ, 135^\circ)$, and (2.07, 1.06) for $\psi_2^{i,o} = (45^\circ, -45^\circ)$. Both the $\psi_2^{i,o} = (45^\circ, 135^\circ)$ and $\psi_2^{i,o} = (45^\circ, -45^\circ)$ methods achieve a higher level of fat suppression than FS-ATR and LCSSFP. Furthermore, the $\psi_2^{i,o} = (45^\circ, -45^\circ)$ pair performs better because of its broad stop-band. The following mean blood-to-muscle (CNR, contrast) values were measured: (9.95, 2.50) for FS-ATR, (13.63, 2.53) for LCSSFP, (11.6, 2.71) for $\psi_2^{i,o} = (45^\circ, 135^\circ)$, and (12.71, 2.74) for $\psi_2^{i,o} = (45^\circ, -45^\circ)$. All methods yield similar blood-to-muscle contrast; however, LCSSFP provides slightly higher SNR than the other methods as indicated by the higher CNR.

The maximum fat-to-muscle (CNR, contrast) measured at 3 T were: (25.97, 7.03) for FS-ATR, (18.65, 4.96) for $\psi_2^{i,o} = (135^\circ, 225^\circ)$, and (6.94, 2.27) for $\psi_2^{i,o} = (45^\circ, -45^\circ)$. The blood-to-muscle (CNR, contrast) pairs were as follows: (17.48, 3.30) for FS-ATR, (25.30, 3.96) for $\psi_2^{i,o} = (135^\circ, 225^\circ)$, and (19.46, 3.15) for $\psi_2^{i,o} = (45^\circ, -45^\circ)$. Similar blood-to-muscle contrast is observed with all methods; however, the $\psi_2^{i,o} = (135^\circ, 225^\circ)$ method yields the highest SNR as expected.

Discussion and Conclusion

We proposed a multiple-acquisition fat-water separation method comprising in-phase and out-of-phase ATR SSFP images. The increased homogeneity of the in-phase and out-of-phase profiles compared to regular SSFP yields effective stop-band suppression with minimal remnant signal. The proposed method achieves better fat suppression than the single-acquisition ATR SSFP method, and outperforms LCSSFP at relatively high flip angles.

Acquisitions with modified spectral responses have been widely used for fat-water separation or fat suppression purposes in SSFP imaging. A disadvantage of the spectrally selective acquisitions is the restriction on possible TRs. LCSSFP is limiting in this sense, with an optimal TR of 2.3 ms at 1.5 T. Although longer TRs can be prescribed, the

sensitivity to field inhomogeneity will be increased. In contrast, methods comprising ATR SSFP acquisitions do not incur the stringent limitations of LCSSFP on TR.

Even though the spectrally-shaped stop-bands are usually broad, the remnant stop-band signal can be significant in single-acquisition methods like FS-ATR. Multiple-acquisition spectrally-selective methods achieve superior suppression compared to these methods. The $\psi_2^{i,o} = (45^\circ, 135^\circ)$ pair outperforms FS-ATR; however, regions of poor fat suppression can be seen in the lower leg images as a result of the residual stop-band signal. When the field-inhomogeneity variation exceeds the width of the $\psi_2^{i,o} = (45^\circ, 135^\circ)$ stop-band, the $\psi_2^{i,o} = (45^\circ, -45^\circ)$ method can be used at the expense of slightly reduced SNR.

A drawback of the proposed method, like any multiple-acquisition method, is the lengthened minimum scan time. In addition, the sequential acquisition of the images may increase the susceptibility to artifacts due to patient motion for relatively long scans. When motion related artifacts are significant (e.g., 3D abdominal imaging), image registration might be needed.

Despite these limitations, the proposed method extends the applicability of fat-suppressed SSFP imaging by allowing a a wide range of imaging parameter selections. Applications such as cardiac imaging and angiography, where high flip angles are used, may benefit from the improved performance of the method. Increased immunity of the stop-band suppression to off-resonant frequency variation can be favorable for high-field and 3D imaging. Furthermore, any imaging application - where large field inhomogeneity is expected - would greatly benefit from this method without the need for long and complex shimming procedures.

Acknowledgments

This work was supported by National Institutes of Health (NIH) under Grant R01 HL039297, Grant R01 HL075803 and by GE Healthcare. The work of Tolga Çukur was supported by a Rambus Corporation Stanford Graduate Fellowship.

References

[1]. Carr HY. Steady-state free precession in nuclear magnetic resonance. Phys Rev. 1958; 112:1693–1701.

[2]. Oppelt A, Graumann R, Barfuss H, Fischer H, Hartl W, Shajor W. FISP - a new fast MRI sequence. Electromedica. 1986; 54:15–18.

[3]. Hawkes RC, Patz S. Rapid Fourier imaging using steady-state free precession. Magn Reson Med. 1987; 4:9–23. [PubMed: 3821484]

[4]. Scheffler K, Heid O, Hennig J. Magnetization preparation during the steady-state: Fat-saturated 3D true FISP. Magn Reson Med. 2001; 45:1075–1080. [PubMed: 11378886]

[5]. Paul D, Hennig J, Zaitsev M. Intrinsic fat suppression in TIDE balanced steady-state free precession imaging. Magn Reson Med. 2006; 56:1328–1335. [PubMed: 17089365]

[6]. Hargreaves BA, Vasanawala SS, Pauly JM, Nishimura DG. Characterization and reduction of the transient response in steady-state MR imaging. Magn Reson Med. 2001; 46:149–158. [PubMed: 11443721]

[7]. Hargreaves BA, Vasanawala SS, Nayak KS, Hu BS, Nishimura DG. Fat-suppressed steady-state free precession imaging using phase detection. Magn Reson Med. 2003; 50:210–213. [PubMed: 12815698]

[8]. Wieben, O.; Leupold, J.; Mannson, S.; Hennig, J. Multi-echo balanced SSFP imaging for iterative Dixon reconstruction; Proceedings of the 13th Annual Meeting of ISMRM; Miami Beach. 2005; p. 2386

[9]. Vasanawala SS, Pauly JM, Nishimura DG. Fluctuating equilibrium MRI. Magn Reson Med. 1999; 42:876–883. [PubMed: 10542345]

[10]. Vasanawala SS, Pauly JM, Nishimura DG. Linear combination steady-state free precession MRI. Magn Reson Med. 2000; 43:82–90. [PubMed: 10642734]

[11]. Hardy, CJ.; Dixon, WT. Steady-state free precession imaging with inherent fat suppression; Proceedings of the 10th Annual Meeting of ISMRM; Honolulu. 2002; p. 473

[12]. Overall WR, Nishimura DG, Hu BS. Steady-state sequence synthesis and its application to efficient fat-suppressed imaging. Magn Reson Med. 2003; 50:550–559. [PubMed: 12939763]

[13]. Absil J, Denolin V, Metens T. Fat attenuation using a dual steady-state balanced-SSFP sequence with periodically variable flip angles. Magn Reson Med. 2006; 55:343–351. [PubMed: 16402382]

[14]. Leupold J, Hennig J, Scheffler K. Alternating repetition time balanced steady state free precession. Magn Reson Med. 2006; 55:557–565. [PubMed: 16447171]

[15]. Vasanawala SS, Hargreaves BA, Pauly JM, Nishimura DG, Beaulieu CF, Gold GE. Rapid musculoskeletal MRI with phase-sensitive steady-state free precession: Comparison with routine knee MRI. AJR Am J Roentgenol. 2004; 184:1450–1455. [PubMed: 15855095]

[16]. Deshpande VS, Shea SM, Laub G, Simonetti OP, Finn JP, Li D. 3D magnetization-prepared True-FISP: A new technique for imaging coronary arteries. Magn Reson Med. 2001; 46:494–502. [PubMed: 11550241]

[17]. Bangerter, NK.; Hargreaves, BA.; Brittain, JH.; Hu, B.; Vasanawala, SS.; Nishimura, DG. 3D fluid-suppressed T2-prep flow-independent angiography using balanced SSFP; Proceedings of the 12th Annual Meeting of ISMRM; Kyoto. 2004; p. 11

[18]. Maki JH, Wilson GJ, Eubank WB, Glickerman DJ, Millan JA, Hoogeveen RM. Navigator-gated MR angiography of the renal arteries: A potential screening tool for renal artery stenosis. AJR Am J Roentgenol. 2007; 188:540–546. [PubMed: 17242266]

[19]. Nayak KS, Lee HL, Hargreaves BA, Hu BS. Wideband SSFP: Alternating repetition time balanced steady state free precession with increased band spacing. Magn Reson Med. 2007; 58:931–938. [PubMed: 17969129]

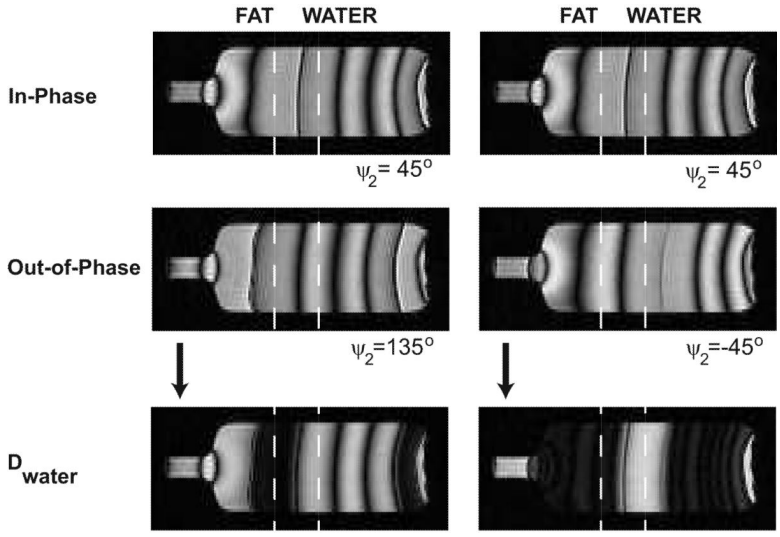

Figure 1.

a: The in-phase $\left(\psi_2^i=45^\circ\right)$ and out-of-phase $\left(\psi_2^i=135^\circ\right)$ magnetization profiles for the frequency range [-600 200] Hz, α = 60°, and TR1/TR2/TE = 3.45/1.15/1.725 ms assuming T1/T2 = 1000/200 ms. Note the phase difference between the out-of-phase and in-phase profiles at -220 Hz. **b:** The summation and subtraction of the in-phase and out-of-phase profiles after compensation for the phase difference yield the water-only and fat-only spectra respectively. **c:** The in-phase $\left(\psi_2^i=45^\circ\right)$ and out-of-phase $\left(\psi_2^o=-45^\circ\right)$ magnetization profiles. **d:** The corresponding water-only and fat-only spectra.

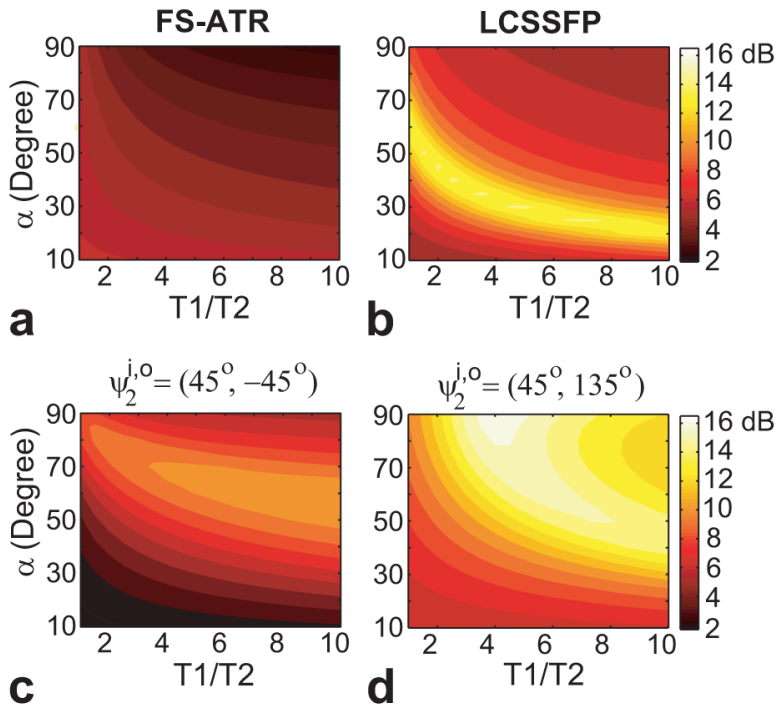

Figure 2.

The ratio of the average pass-band signal to the average stop-band signal was simulated for a range of T1/T2 ratios, flip angles and various suppression methods: (displayed in logarithmic scale) **a:** FS-ATR, **b:** LCSSFP, **c:** $\psi_2^{i,o} = (45^\circ, -45^\circ)$ and **d:** $\psi_2^{i,o} = (45^\circ, 135^\circ)$. The proposed method $\left(\psi_2^{i,o} = (45^\circ, 135^\circ)\right)$ achieves better suppression than LCSSFP for the whole range of simulation parameters except in the small vicinity of $\alpha = 30°$. The performance of the proposed method improves with increasing flip angle. The signal ratio of FS-ATR is lower compared to the multiple-acquisition methods.

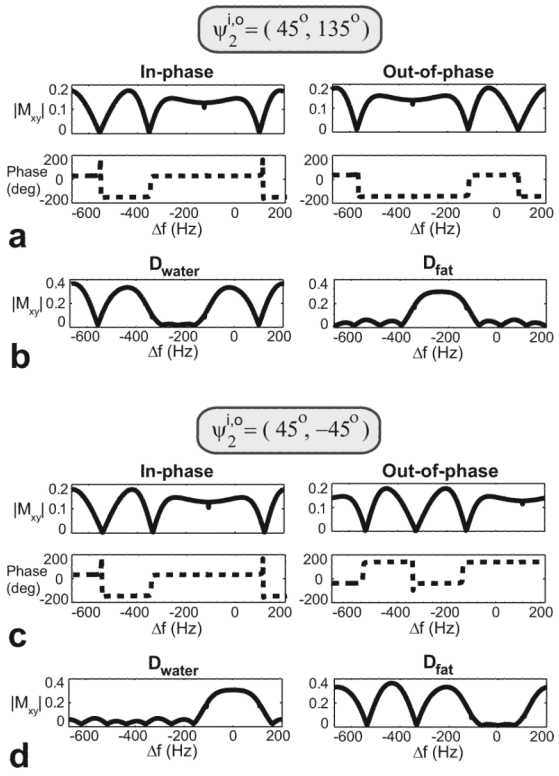

Figure 3.

Phantom images were acquired with out-of-phase and in-phase 3D ATR SSFP profiles, where off-resonance was generated with a linear field gradient across the readout direction (horizontal). Water images were reconstructed from the two sets of in-phase and out-of-phase images with the corresponding ψ_2 pairs, $\psi_2^{i,o} = (45^\circ, 135^\circ)$ and $\psi_2^{i,o} = (45^\circ, -45^\circ)$. The $\psi_2^{i,o} = (45^\circ, -45^\circ)$ pair creates a broader stop-band.

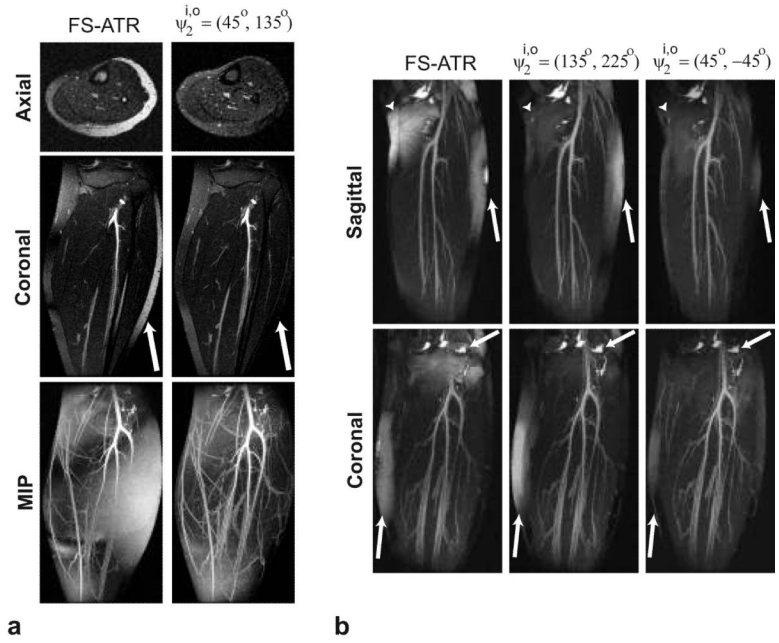

Figure 4.

Comparison of FS-ATR and the proposed method at two different field strengths: **a**: 1.5 T, **b**: 3 T. **a**: Coronal and axial slices for the FS-ATR and $\psi_2^{i,o} = (45^\circ, 135^\circ)$ acquisitions at 1.5 T are displayed along with the corresponding MIPs. The arrows point to the region where the proposed method achieves better fat suppression than the FS-ATR method. Improved fat suppression of the proposed method results in superior depiction of the vasculature in the MIPs. However, regions with visible residual fat signal still exist in the images produced with the proposed method as a result of the remnant stop-band signal. **b**: Sagittal and coronal thin slab MIPs of the calf acquisitions at 3 T are displayed for the FS-ATR ($\psi_2 = 180°$), $\psi_2^{i,o} = (135^\circ, 225^\circ)$ and $\psi_2^{i,o} = (45^\circ, -45^\circ)$ methods. The $\psi_2^{i,o} = (135^\circ, 225^\circ)$ combination achieves better fat suppression than FS-ATR. However, the range of off-resonant frequency variation limits the amount of fat suppression. The $\psi_2^{i,o} = (45^\circ, -45^\circ)$ combination achieves the highest level of fat suppression due to its broad stop-band.

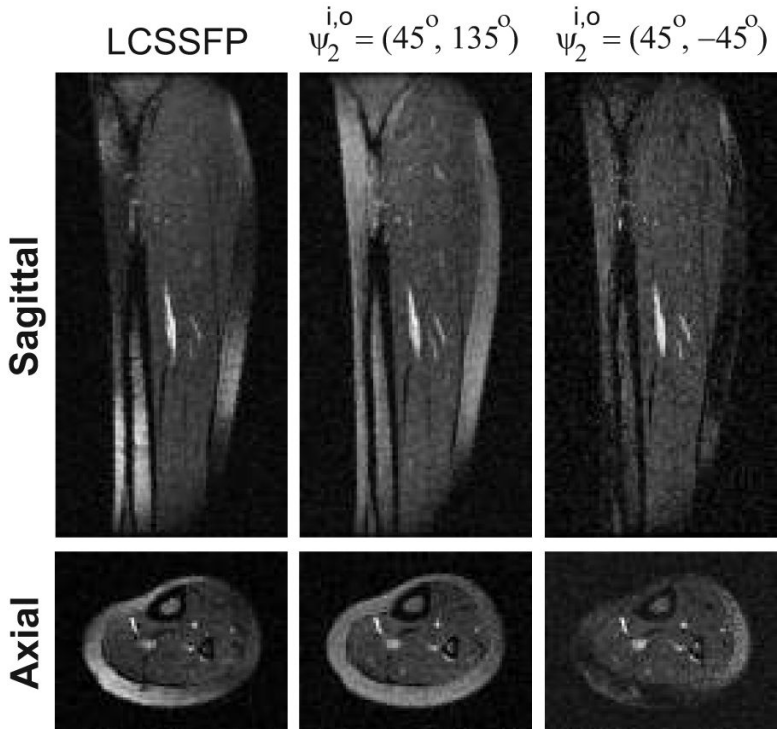

Figure 5.

Sagittal and axial calf images are shown for LCSSFP, and the $\psi_2^{i,o} = (45^\circ, 135^\circ)$ and $\psi_2^{i,o} = (45^\circ, -45^\circ)$ pairs. The $\psi_2^{i,o} = (45^\circ, -45^\circ)$ method achieves the highest level of suppression, at the expense of a lower SNR.